Available online at www.sciencedirect.com
SCIENCE DIRECT®
International Journal of Mass Spectrometry 233 (2004) 325–333
International Journal of Mass Spectrometry
www.elsevier.com/locate/ijms

Discrimination effects for ions with initial kinetic energy produced by electron ionization of C_2H_2 in a Nier-type ion source

S. Feil, A. Bacher, M. Zangerl, W. Schustereder, K. Gluch, P. Scheier*

Institut für Ionenphysik, Leopold Franzens Universität, Technikerstr. 25, Innsbruck A-6020, Austria

Received 1 December 2003; accepted 8 January 2004

Abstract

Fully three-dimensional (3-D) ion trajectory simulations of a Nier-type ion source were performed for mono-energetic ions with a spatial resolution of the potential array of 0.1 mm. Experimentally determined ion beam profiles were fitted with a superposition of simulated ion beam profiles in an effort to determine the initial ion kinetic energy distribution and the extraction efficiency from the ion source for a given product ion. This method allows the analysis of ion beam profiles of highly energetic fragment ions that are affected by a reduced ion extraction efficiency. As an example, ion beam profiles of product ions formed by electron impact ionization of acetylene (C_2H_2) at an electron energy of 100 eV were analyzed with the present method as well as with a method developed by Poll et al. [Int. J. Mass Spectrom. Ion Process. 112 (1992) 1], which is based essentially on a simplified two-dimensional (2-D) ion trajectory analysis. For highly energetic fragment ions, the results obtained by the two methods differ by as much as 84%.

Keywords: Ionization cross sections; Excess kinetic energy; Fragment ions; Ion discrimination

1. Introduction

Dissociative ionization of molecules induced by electron impact is of significance in many different areas such as low-temperature plasmas, radiation chemistry, mass spectrometry, chemical analysis, and edge plasmas in fusion reactors [1–5]. The kinetic energy distribution of ionic and neutral fragments produced via dissociative ionization can have a profound impact on the energy deposition and the energy transfer pathways in these media, in particular when energetic fragments with kinetic energies of several electronvolts are present. The modeling of environments where dissociative ionization processes are important requires knowledge not only of the production efficiency of the various fragment ions, but also of their kinetic energy distribution. Furthermore, different pathways leading to the formation of the same fragment ion may have different threshold energies and different exothermicities. Thus, the kinetic energy distribution for a given fragment ion often depends strongly on the electron energy.

Fragment ions that are formed with high kinetic energies often are collected with a substantially reduced efficiency compared to thermal or near-thermal fragment ions. This, in turn, has a strong influence on the partial ionization cross section values that are determined [6–9]. Measurements of absolute partial and total ionization cross sections of molecules are now routinely carried out using instruments that were designed and constructed specifically to ensure complete ion collection or at least a uniform ion collection efficiency [10,11]. Even in cases where a complete ion collection cannot be accomplished, reliable ionization cross sections can be obtained, if the so-called discrimination factor for energetic fragment ions is determined, i.e., if the fraction of ions that are collected is accurately known. For a conventional double-focusing mass spectrometer equipped with a modified Nier-type ion source, Poll et al. [6] demonstrated that ion trajectory calculations of the extraction region of the ion source allow the determination of the ion loss (or discrimination factor). In such an instrument, which is schematically shown in Fig. 1, information about the kinetic energy of the ions produced in the ion source can be obtained by applying a deflection voltage to the ion beam extracted from the ion source in the *z*-direction (see Fig. 1). The ion motion in the *z*-direction is influenced very little by

* Corresponding author. Tel.: +43-512-507-6243; fax: +43-512-507-2932.
E-mail address: paul.scheier@uibk.ac.at (P. Scheier).

1387-3806/$ – see front matter © 2004 Elsevier B.V. All rights reserved.
doi:10.1016/j.ijms.2004.01.013

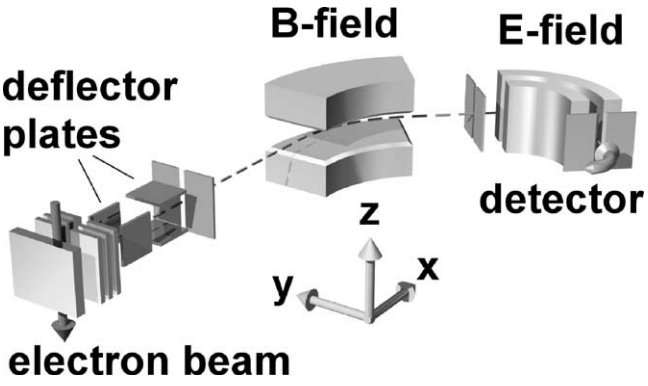

Fig. 1. Schematic view of the experimental setup.

the ion optical properties of the extraction and acceleration electrodes. Sen Sharma and Franklin [12] demonstrated that the measured deflection profiles in the *z*-direction (*z*-profiles) can be used to determine the translational energies of fragment ions and that the results are in good agreement with those obtained from other methods, such as a retarding potential analysis (see also earlier references given in [12]). The initial kinetic energy of an ion in the *z*-direction is proportional to the square of the deflection voltage in that direction. The proportionality constant can either be determined empirically by normalization to ions of known kinetic energy or it can be calculated/modeled for a given specific experimental arrangement [13]. For the present set-up, this constant was determined previously to be roughly 10^{-3} [6,14,15]. The first derivative of the ion signal as a function of the deflection voltage yields the kinetic energy distribution after proper normalization of the energy axis. However, this method assumes that ions of different kinetic energies contribute equally to the measured ion signal, which is generally not the case as the ion detection efficiency for energetic fragment ions can be significantly less than that for the parent ions [15]. A major concern regarding the accuracy of the results from the ion trajectory simulations using the method of Poll et al. [6,15] is the fact that in their model the initial ion kinetic energy (average value as well as the entire energy distribution) are derived from *z*-profiles, which are affected by the reduced extraction efficiency for energetic fragment ions. Furthermore, due to computational limitations their simulations assumed a simplified, essentially two-dimensional (2-D) geometry, either using infinitely high slits (planar symmetry) or circular holes (cylinder symmetry) instead of finite slits and a comparatively coarse spatial resolution of the potential array of 0.5 mm, which was comparable to the distance between the first two extraction lenses.

In the present work, we use a different approach to determine the initial ion kinetic energy distribution. Ion beam profiles are calculated for a set of fragment ion energies using fully three-dimensional (3-D) ion trajectory simulations with a spatial resolution of the potential array of 0.1 mm. A fit of the complete set of calculated *z*-profiles to the experimentally determined *z*-profiles yields directly the initial kinetic energy distribution. Hydrocarbon molecules are known to form fragment ions with broad kinetic energy distributions ranging from thermal energies to many electronvolts [6,13,16–18]. This effect is especially important for light fragment ions such as H^+ and $H_2{}^+$ as a result of momentum conservation. The fragment ions of C_2H_2 served as a test of the present method and a comparison of our present results with those obtained from the method of Poll et al. [6,15] is made.

2. Ion trajectory simulations

The geometric dimensions of all elements of our Nier-type ion source were carefully determined from the completely disassembled parts with an accuracy of 0.1 mm. Fig. 2 shows the ion source housing, the pusher electrode, the filament Wehnelt, and the electron collector. The separation between the various lenses is not to scale in Fig. 2 in order to facilitate a better view of the details of the geometry of the lenses. The voltages applied to each lens were measured in situ with a digital voltmeter under conditions that were iden-

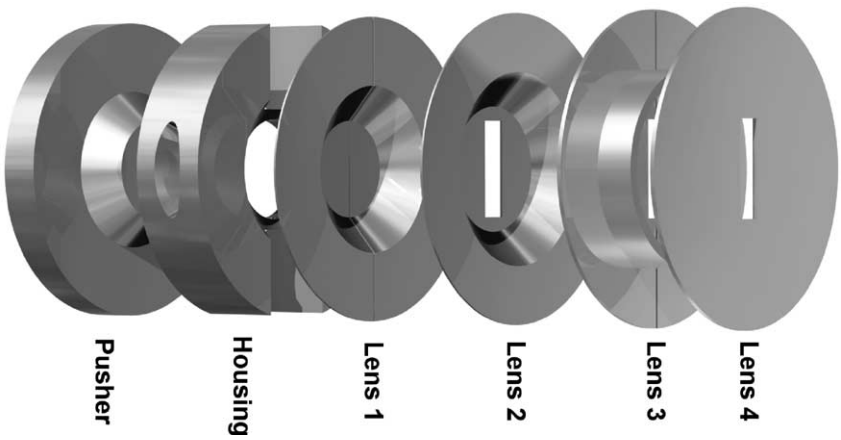

Fig. 2. Design of the present ion source. The distance between the different lenses is increased for a better view of the details. Please note the narrow slit (0.6 mm) between the two parts of lens 1. Most of the ions are lost by neutralization at this lens.

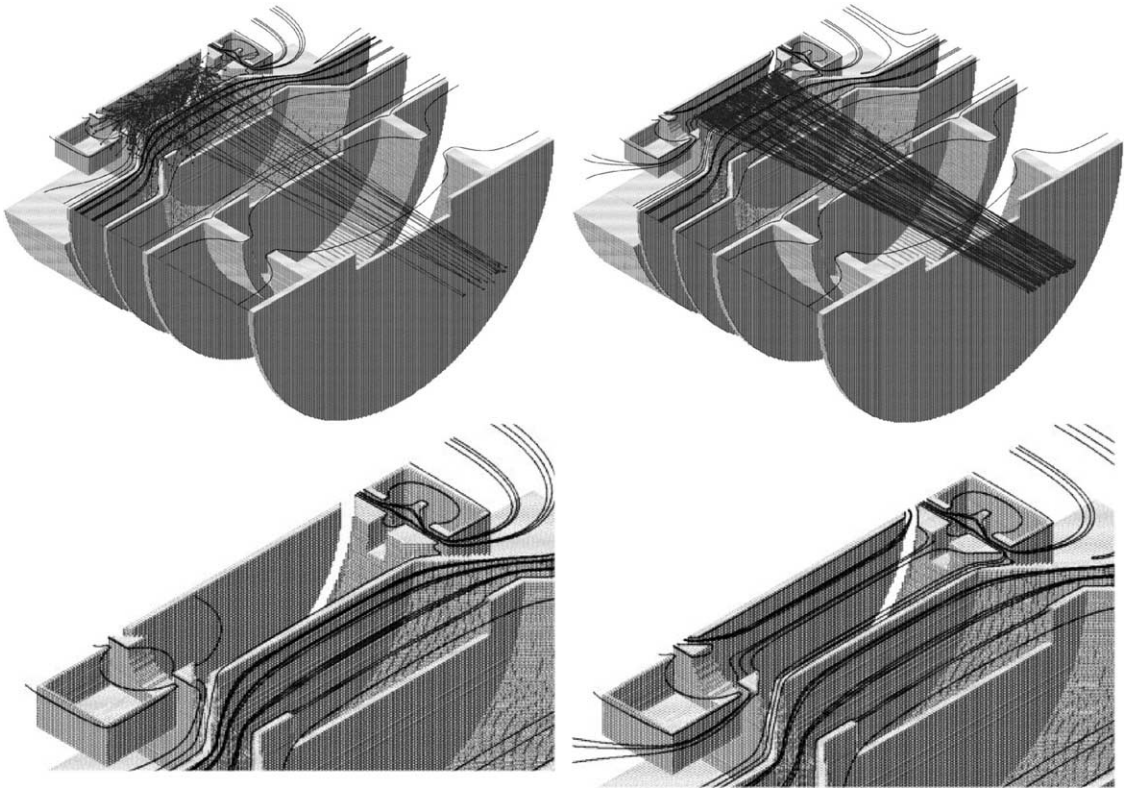

Fig. 3. Results of ion trajectory simulations of the present ion source. Only half of the ion source is shown. On the left side, a weak penetrating field is used to extract the ions from the ion source and on the right side, a homogeneous electric field formed with the pusher and lens 1 (3 kV/m) is used to extract more ions from the source. The direction of the electrostatic field is indicated by some contour lines. In the two upper panels, the trajectories of 500 ions are shown.

tical to those during the actual experiments. The electrostatic potential between the electrodes was calculated by SIMION [19] with an accuracy of better than 0.1 mV. Fig. 3 shows a cross sectional cut through the center of the ion source in the (x, z) plane. In addition to 500 individual ion trajectories, some contour lines of the electrostatic potential are also shown. On the left side, a weak penetrating field is used for the ion extraction, whereas, on the right side, the pusher and the first two lenses generate a higher homogeneous electric field in the ion source housing that extracts ions much more efficiently. The initial kinetic energy of the fragment ions in this simulation was 1 eV. The filament was held 100 V below the potential of the ion source housing (resulting in an electron energy of 100 eV) and the Wehnelt was at 100 V higher than the potential of the ion source. The small size of the aperture, where the electrons enter the ion source housing, reduces the influence of field penetration caused by the filament and Wehnelt potentials, so that the potential on the other side of the ion source is practically unperturbed. In contrast, the aperture, where the electrons leave the ion source and are collected in a Faraday cup, is much larger. Since the Faraday cup that is held at a potential that is 24 V higher than that of the ion source, field penetration through this aperture perturbs the potential in the ion source housing close to the aperture substantially. The effect of the Faraday cup bias on the ion trajectories is especially strong in the case of a weak penetrating extraction field. Ions that are generated close to the opening of the Faraday cup are pushed to the center of the ion source and towards the extraction slit. These ions gain an additional velocity in the z-direction and generate a spurious peak in the z-profile. Fortunately, this peak appears only on one side of the z-profile and is well separated from the regular peak. Ion beam profiles for different initial kinetic energies of the ions were simulated for a weak penetrating field and for a homogeneous extracting field using 2×10^6 ion trajectories with ions generated at random positions inside the ion source along the path of the electron beam (which has a width of about 1 mm and is guided by weak homogeneous magnetic field) with initial velocity vectors that were uniformly distributed over the full solid angle. The discrimination factor can easily be determined as the fraction of ions that are transported through the entire system of lenses and deflection plates (see Fig. 1) to the total number of ions initially used for the simulation.

Fig. 4 shows simulated z-profiles for initial kinetic energies of 0, 0.05, 0.1, 0.5, 1, 5, and 10 eV and a strong extraction field. Without ion discrimination, a z-profile of a mono-energetic ion beam has a rectangular shape (see the 0 eV line in Fig. 4). The major ion losses occur at the narrow slit between the first two extraction lenses, which are 0.6 mm apart. If the initial velocity component of an ion in the y-direction (perpendicular to the extraction slit) exceeds

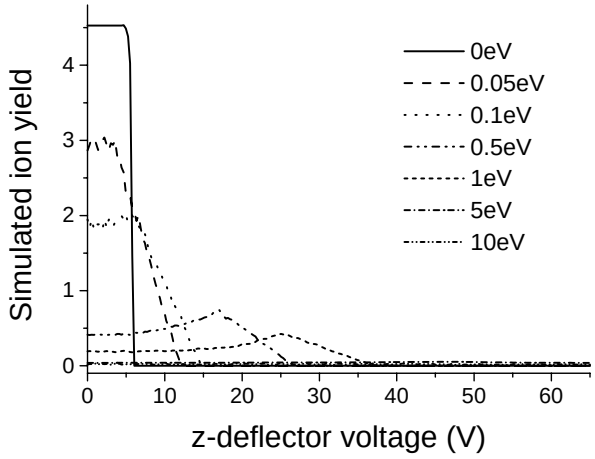

Fig. 4. Simulated *z*-profiles for different initial ion kinetic energies.

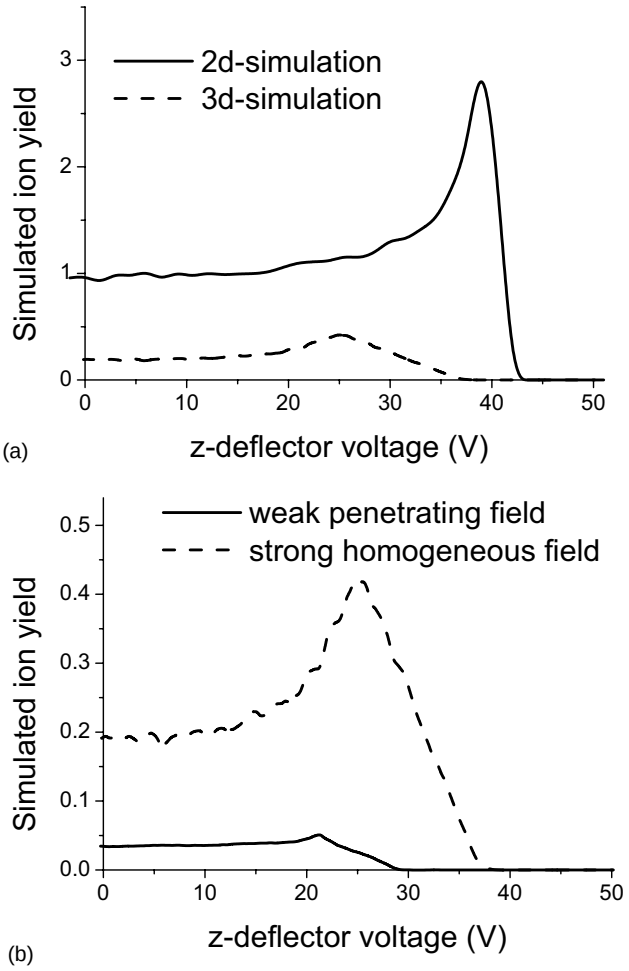

Fig. 5. Top panel: calculated *z*-profiles for 2-D simulation (dashed line according to Gluch et al. [21]) in comparison to a present 3-D simulation. An initial ion kinetic energy of 1 eV was used. Bottom panel: the influence of high (strong homogeneous electric field) and low (weak penetrating field) extraction voltage on the shape of the simulated *z*-profiles. Again, the ions started with an initial kinetic energy of 1 eV.

a certain value, the ion will hit these extraction lenses. Since ions that start parallel to the *y*-direction have only a small velocity component in the *z*-direction, it is primarily the center of the *z*-profile that is affected by this ion loss process. For ion energies larger than 0.5 eV, the simulated *z*-profiles all reveal a local minimum at the center (see Fig. 4). The earlier 2-D ion trajectory simulations of Poll et al. [15], which used a geometry, where the ion source was approximated by a planar geometry with infinitely long lenses in the *z*-direction, showed a similar ion loss. However, for large *z*-deflection voltages, the *z*-profiles in the 2-D simulations differ substantially from the present results (see Fig. 5a). An ion that starts with a high initial velocity in the *z*-direction will always be extracted from an ion source with infinitely high slits. However, in reality, such an ion will hit the ion source housing before it reaches the extraction lens. Thus, the expected steep shoulder of the *z*-profile in the case where there is no ion discrimination in the *z*-direction will change to a smooth onset and a shift of the maximum towards lower deflection voltages in the *z*-direction. For weak penetrating field extraction, this effect is observed already for very low initial kinetic energies. For high extraction fields, the ion loss in both directions is reduced and the shape of the *z*-profile is closer to a rectangle (see Fig. 5b).

3. Experimental details

The apparatus used in the present experiment is a double focusing Nier–Johnson two-sector-field mass spectrometer of reversed geometry with a Nier-type electron impact ion source (see Fig. 1) and has been described in detail in earlier publications [6,14]. A stagnant gas target is crossed by a well-characterized, magnetically collimated electron beam with a FWHM energy spread of ∼0.5 eV. Acetylene of 99.9% purity was used. Product ions were extracted from the ion source either by a weak penetrating electric field (typically 50 V/m) or by a strong homogeneous electric field (3 kV/m) and accelerated to 3 kV. Before entering the mass spectrometer through a narrow entrance slit, the ions pass two pairs of perpendicular deflection plates that allow a steering of the ion beam in two directions. For cross section measurements, the deflection plates are used to sweep the ion beam across the entrance slit [20] and the cross section is obtained from the integrated ion signal. In all other modes of operation, the deflection plates are kept at fixed voltages that maximize the ion flux into the mass spectrometer. After passing through a magnetic sector field and an electric sector field, the ions are detected by a secondary electron multiplier operated in a pulse counting mode. Since a weak penetrating field cannot extract fragment ions that have initial kinetic energies in the *z*-direction larger than 100 meV (see the ion trajectory simulations in Fig. 2), a strong homogeneous electric field capable of extracting ions with initial kinetic energies up to several eV in the *z*-direction had to be used in most studies carried out as part of this work.

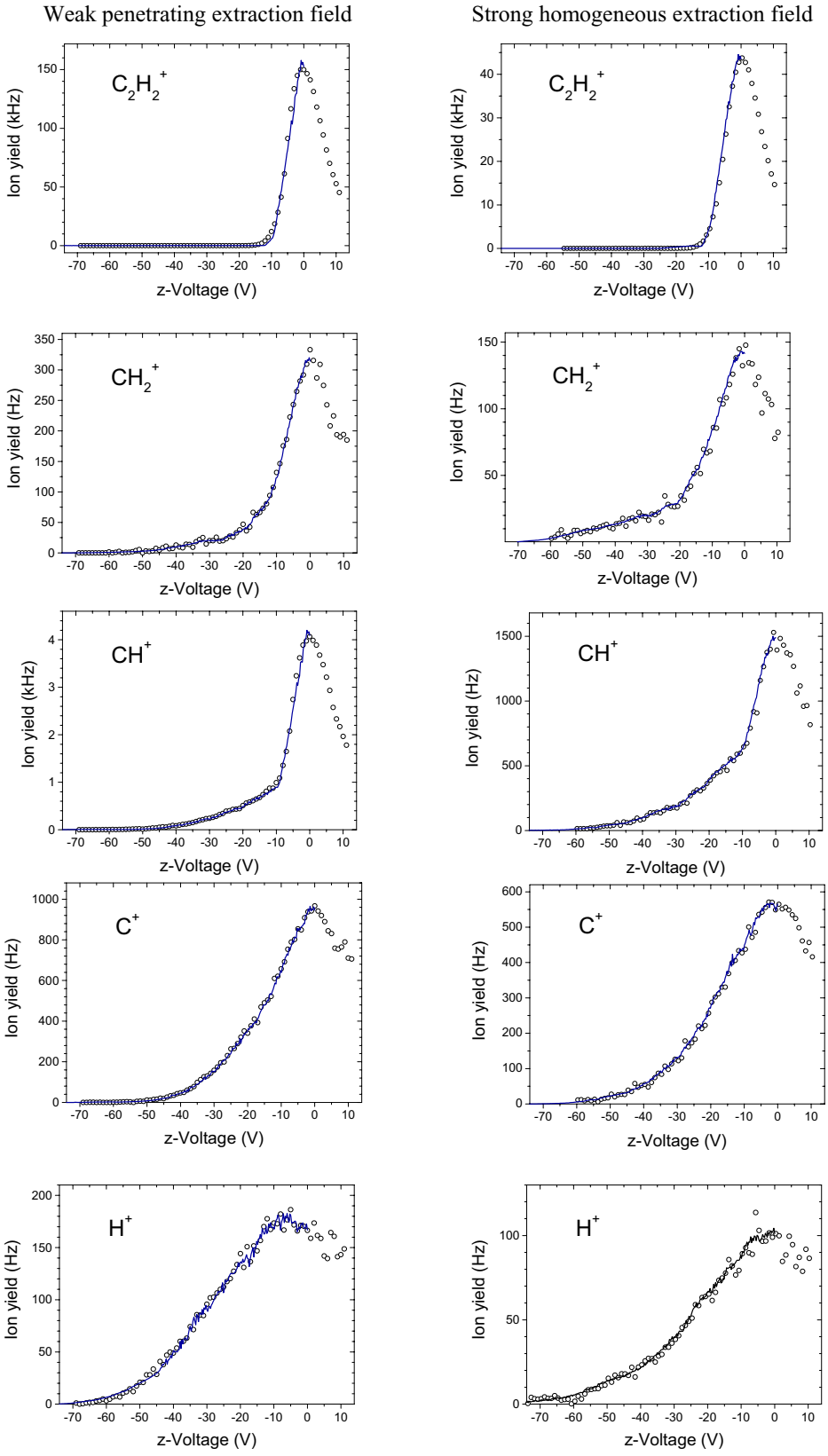

Fig. 6. Left half of the *z*-profiles of several product ions of C_2H_2 formed by electron impact ionization at an electron energy of 100 eV. The open circles are the experimental data. The solid line are the best fits to the experiments derived by a superposition of a set of simulated *z*-profiles (for a few initial energies these simulated *z*-profiles are shown in Fig. 3).

4. Results and discussion

The experimentally determined *z*-profiles for all product ions formed by electron impact ionization of C_2H_2 at an electron energy of 100 eV are shown in Fig. 6 as open circles. The solid line represents the best fit to the experimental data. This fit is obtained iteratively using a set of simulated *z*-profiles for 57 different ion kinetic energies (in steps of 0.05 eV between 0 and 2 eV and in steps of 0.5 eV from 2.5 to 10 eV) utilizing 2×10^6 individual ion trajectories at each energy. The kinetic energy distribution can be determined directly by plotting the weighting factors as a function of the ion kinetic energy of each simulated *z*-profile. Poll et al. [6] determined the kinetic energy distribution by plotting the first derivative of the *z*-profile as a function of the properly normalized square of the deflection voltage. The kinetic energy distribution functions resulting from the present method (solid lines) are compared in Fig. 7 to those obtained from the method described in Ref. [6] (dashed lines). The dotted line in each diagram was derived by multiplication of the dashed line with the presently determined reciprocal relative ion extraction efficiency shown in Fig. 8. It is apparent that the two methods yield different ion kinetic energy distributions for all ions studied. The discrepancies become more

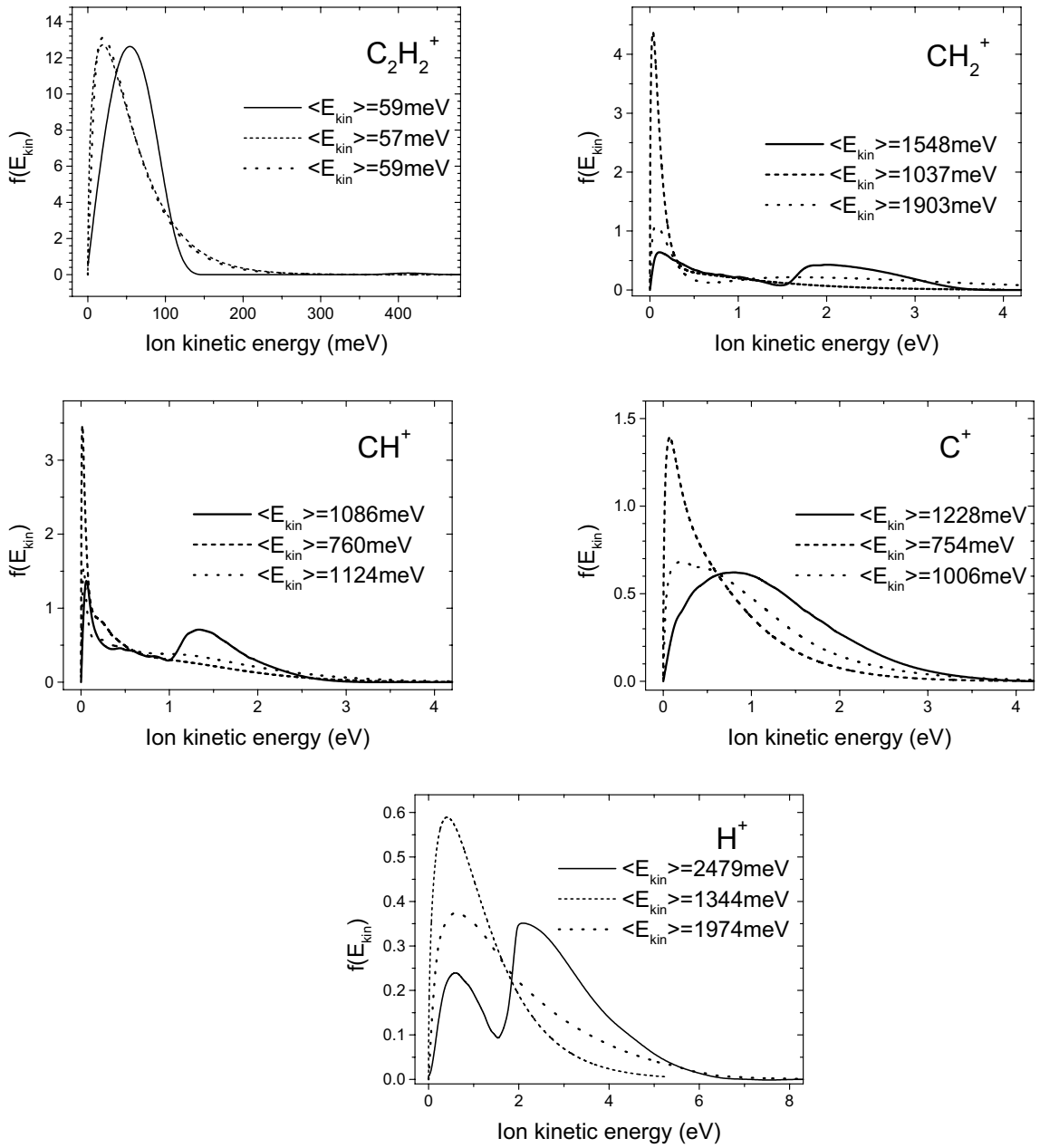

Fig. 7. Ion kinetic energy distributions for different product ions of acetylene. The solid line corresponds to the analysis of the *z*-profiles (shown in Fig. 6) according to the present method. The dashed line was derived according to the method developed by Poll et al. [6,15] and the dotted line was derived by dividing the dashed line with the presently determined relative ion extraction efficiency shown in Fig. 8.

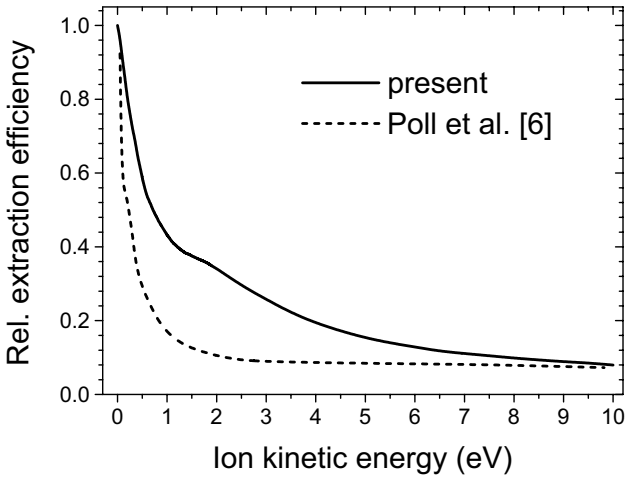

Fig. 8. Relative ion extraction efficiency curves for the 2-D simulations of Poll et al. [6] and the present 3-D simulations. The data were normalized to the extraction efficiency of ions having no initial kinetic energy.

pronounced for lighter fragment ions, which have generally broader energy distributions and a higher fraction of energetic fragment ions.

It is often illustrative to decompose a measured and/or simulated kinetic energy distribution into components corresponding to groups of ions that can be represented by specific average kinetic energy values. Such groups often represent ions that were produced by the same (dissociative ionization) process. Each group of ions can be described by a Gaussian function with a certain width about a center, whose position is related to the average kinetic energy of that group of ions. In the *z*-profiles (see Fig. 9, top), the various groups of ions are represented either by a pure Gaussian function (indicative of thermal or near-thermal ions) or by flat-topped Gaussian functions (which correspond to Boltzmann energy distributions that are shifted to higher energy and thus describe energetic, non-thermal ions in the distribution; see Fig. 9, bottom). Fig. 9 shows a fit of the CH^+ *z*-profile with three curves. The total kinetic energy distribution of an ion is given by the sum of all individual contributions (solid line in Fig. 9, bottom). For the fragment ions CH^+ and CH_2^+, the *z*-profiles consist of different parts, a narrow Gaussian-like contribution and a broad feature that resembles the *z*-profiles of the H^+ and C^+ ions. A careful analysis of the mass spectrum of C_2H_2 shows peaks at non-integer masses, 12.5 and 13.5 Da, which originate from the doubly charged ions C_2H^{2+} and $^{13}C^{12}CH_2^{2+}$, respectively. Using the natural abundance of ^{13}C and the ion yield of $^{13}C^{12}CH_2^{2+}$, it is possible to calculate the amount of $^{12}C_2H_2^{2+}$ that has the same mass per charge ratio as the fragment ion CH^+. The narrow peak of the *z*-profile is attributable exclusively to the doubly charged acetylene ion. Furthermore, *z*-profiles measured at different electron energies show that the narrow contribution of the $CH^+/^{12}C_2H_2^{2+}$ peak has the same appearance energy as that of the doubly charged ion $^{13}C^{12}CH_2^{2+}$, which is free from contributions

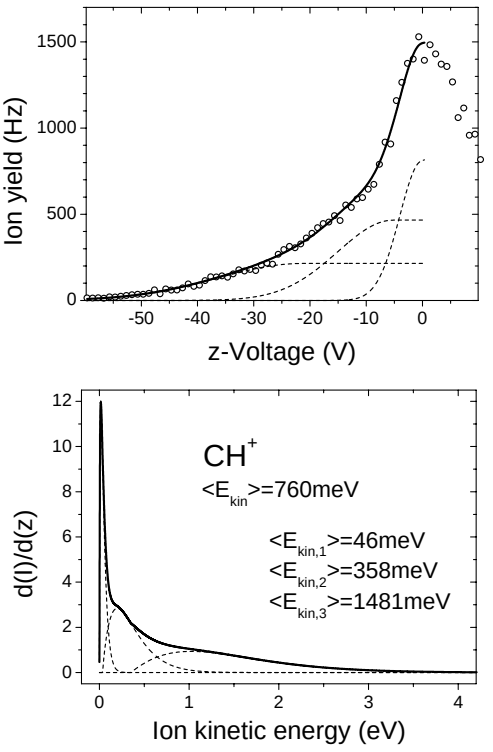

Fig. 9. Analysis of the *z*-profile of CH^+ measured at 100 eV and high extraction field conditions according to the method developed by Poll et al. [6] and later improved by Gluch et al. [21,22].

of singly charged ions. The initial kinetic energy of the ions forming the narrow peak is 46 meV, which is basically the same as for the singly charged parent ion $C_2H_2^+$.

Very similar ion kinetic energy distributions were obtained from the present method and from the method of Poll et al. [6] for all thermal ions, i.e., for singly or doubly charged parent ions and fragment ions that have lost only one H atom. By contrast, the kinetic energy distribution of energetic fragment ions depends strongly on the method used. The average initial kinetic energies obtained from the present 3-D model are typically larger than those from the previous 2-D model by as much as 80%. Furthermore, for the two fragment ions H^+ and CH^+ the kinetic energy distribution at high kinetic energies reveals two contributions in our analysis that cannot be resolved using the earlier method [6]. This large discrepancy in the kinetic energy distributions and the average initial kinetic energies derived from the two methods may suggest that the discrimination factors (i.e., the ion extraction efficiencies at given values of the kinetic energy of the ions formed in the source) that are used to correct the partial cross section curves also depend strongly on the data analysis method. However, this does not seem to be the case for the ions produced from the C_2H_2 molecule as can be seen from Table 1, which lists the average kinetic energies and the fraction of ions extracted from the ion source for all ions obtained by electron impact on C_2H_2 using both methods. According to Poll et al. [6,15] partial cross sections can be corrected for the reduced ion extraction efficiency by mul-

Table 1
Average initial ion kinetic energies and extraction efficiencies obtained by the analysis of the *z*-profiles of several product ions of acetylene formed by electron impact ionization at an electron energy of 100 eV

Ion	Present		Poll et al. [6]	
	$\langle E_{kin} \rangle$	Extraction efficiency	$\langle E_{kin} \rangle$	Extraction efficiency
H^+	2479	0.38	1344	0.38
C^+	1228	0.50	754	0.51
CH^+	1086	0.53	760	0.60
CH_2^+	1548	0.52	1037	0.59
$C_2H_2^+$ (a)	59	0.92	57	0.95
$C_2H_2^+$ (b)	45	0.88	44	0.97

Product ions were extracted from the ion source by a strong homogeneous electric field except for the last line designated $C_2H_2^+$ (b) where instead a weak penetrating electric field was used. The average initial ion kinetic energies were calculated from the ion kinetic energy distributions shown in Fig. 7. The ion extraction efficiency is a direct result of the present method. In contrast, the values given in the last column were deduced from the relative extraction efficiency curve based on the present 3-D simulations shown in Fig. 8 (solid line).

tiplying the ion yield with a discrimination factor that has been determined from ion trajectory simulations at the average initial kinetic energy of the corresponding product ion. The present determination of the ion kinetic energy distribution using a set of simulated *z*-profiles automatically yields directly also the discrimination factor. Fig. 8 shows the discrimination factor determined from the present 3-D analysis as a function of the initial ion kinetic energy (solid line) in comparison with the discrimination factor obtained from the 2-D ion trajectory simulations of Poll et al. [15] (dashed line). It is apparent that the 2-D simulations result in an ion extraction efficiency that declines much more rapidly as the ion kinetic energy increases. As shown in Fig. 7, the initial ion kinetic energy distributions determined by the present method differ substantially from the results obtained by the method of Poll et al. [6] and the average ion kinetic energies determined from the present method are systematically larger than those from [6] (Table 1). Nevertheless, the ion extraction efficiencies determined with the two methods are very similar, at least for the lighter ions. However, this is only a coincidence caused by the fact that for this particular molecule the lower average kinetic energies for these ions derived from the 2-D simulation are compensated by the particular dependence of the ion extraction efficiency in the 2-D simulation on the ion kinetic energy. A careful inspection of Table 1 for the heavier ions shows that the present method yields consistently lower ion extraction efficiencies. In general, one should expect that both the ion kinetic energies (average values and energy distribution) and the ion discrimination factors depend on the particular simulation and that the present 3-D simulation, as the more rigorous method, yields more reliable results than the 2-D method of Poll et al. [6]. If reliable partial ionization cross sections are to be determined for energetic fragment ions by putting measured relative ion abundances obtained by experimental techniques that are susceptible to ion discrimination on an absolute scale, the present method yields directly the necessary discrimination factor for each ion.

5. Conclusions

A novel method for the analysis of ion beam profiles was developed that accounts quantitatively for reduced ion extraction efficiencies of specific ions from a Nier-type electron impact ion source using a set of calculated *z*-profiles from fully 3-D ion trajectory simulations. A superposition of these curves is fitted in an iterative way to the experimentally determined *z*-profiles. This yields the initial ion kinetic energy distribution of the various ions. Furthermore, it is possible to derive directly the fraction of ions extracted from the ion source. This ion extraction efficiency must be known for each ion in order to determine absolute partial ionization cross sections from relative ion efficiency curves. The *z*-profiles of several product ions of C_2H_2 formed by electron impact ionization at an electron energy of 100 eV were analyzed according to the present method and the results, i.e., initial ion kinetic energy distribution, average initial ion kinetic energy and relative ion extraction efficiency, were compared with the results of a previous 2-D *z*-profile analysis developed by Poll et al. [6,15]. Although the initial ion kinetic energy distributions obtained with the two methods differ substantially, the relative ion extraction efficiency values agree quite well (see Table 1), at least for some ions. However, it is obvious that a fully 3-D analysis of the ion beam profiles according to the present procedure (and data obtained with a retarding potential method) is always preferable and will yield more reliable results in general. Even though the numerical effort is higher, the present method requires no assumptions or approximations.

Acknowledgements

This work has been carried out within the association EURATOM-ÖAW and was supported by the FWF, OENB, and BMWV, Wien, Austria. It is a pleasure to thank Professor T.D. Märk for his valuable comments concerning the subject of this article.

References

[1] L.G. Christophorou (Ed.), Electron Molecule Interactions and their Applications, Academic Press, Orlando, FL, 1984.
[2] T.D. Märk, G.H. Dunn (Eds.), Electron Impact Ionization, Springer, Vienna, 1985.
[3] L.C. Pitchford, B.V. McKoy, A. Chutjian, S. Trajmar (Eds.), Swarm Studies and Inelastic Electron-Molecule Collisions, Springer, New York, 1987.
[4] R.K. Janev (Ed.), Atomic and Molecular Processes in Fusion Edge Plasmas, Plenum, New York, 1995.

[5] J.P. Mohr, W.L. Wiese (Eds.), Atomic and Molecular Data and their Applications, AIP Conference Proceedings, vol. 434, AIP, Woodbury, NY, 1998.
[6] H.U. Poll, V. Grill, S. Matt, N. Abramzon, K. Becker, P. Scheier, T.D. Märk, Int. J. Mass Spectrom. Ion Process. 177 (1998) 143.
[7] H.C. Straub, D. Lin, B.G. Lindsay, K.A. Smith, R.F. Stebbings, J. Chem. Phys. 106 (1997) 4430.
[8] C. Tian, C.R. Vidal, J. Phys. B At. Mol. Opt. Phys. 31 (1998) 895.
[9] B. Adamczyk, A.J.H. Boerboom, B.L. Schram, J. Kistemaker, J. Chem. Phys. 44 (1966) 4640.
[10] H.C. Straub, P. Renault, B.G. Lindsay, K.A. Smith, R.F. Stebbings, Phys. Rev. A 52 (1995) 1115.
[11] C. Tian, C.R. Vidal, J. Chem. Phys. 108 (1998) 927.
[12] D.K. Sen Sharma, J.L. Franklin, Int. J. Mass Spectrom. Ion Process. 13 (1974) 139.
[13] R. Taubert, Z. Naturforschg. 19a (1964) 484;
R. Fuchs, R. Taubert, Z. Naturforschg. 19a (1964) 494;
R. Taubert, Z. Naturforschg. 19a (1964) 911;
R. Fuchs, R. Taubert, Z. Naturforschg. 19a (1964) 1181.
[14] V. Grill, G. Walder, D. Margreiter, T. Rauth, H.U. Poll, P. Scheier, T.D. Märk, Z. Phys. D 25 (1993) 217.
[15] H.U. Poll, C. Winkler, D. Margreiter, V. Grill, T.D. Märk, Int. J. Mass Spectrom. Ion Process. 112 (1992) 1.
[16] J. Apell, C. Kubach, Chem. Phys. Lett. 11 (1971) 486.
[17] R. Locht, J.L. Olivier, J. Momigny, Chem. Phys. 43 (1979) 425.
[18] T. Fiegele, C. Mair, P. Scheier, K. Becker, T.D. Märk, Int. J. Mass Spectrom. 207 (2001) 145.
[19] D.A. Dahl, SIMION 3D, Version 7.0, 2000.
[20] V. Grill, G. Walder, P. Scheier, M. Kurdel, T.D. Märk, Int. J. Mass Spectrom. Ion Process. 129 (1993) 31.
[21] K. Gluch, P. Scheier, W. Schustereder, T. Tepnual, L. Feketeova, C. Mair, S. Matt-Leubner, A. Stamatovic, T.D. Märk, Int. J. Mass Spectrom. 228 (2003) 307.
[22] K. Gluch, S. Feil, P. Scheier, W. Schustereder, T. Tepnual, L. Feketeova, C. Mair, S. Matt-Leubner, A. Stamatovic, T.D. Märk, in: D. Reiter et al. (Eds.), Atoms Plasma Series, Springer, in press.